Fe$_3$O$_4$ magnetic nanoparticles as a catalyst of oxone for the removal of a typical amino acid

Cheng Liu[a,b,*], Meiqi Zhao[b], Siyuan He[b], Zhen Cao[b], Wei Chen[b]

[a]*Key Laboratory of Integrated Regulation and Resource Development on Shallow Lakes, Ministry of Education, Hohai University, Nanjing 210098, China, Tel. +86 18913959968; Fax: +86 25 83787618; email: liucheng8791@hhu.edu.cn (C. Liu)*
[b]*College of Environment, Hohai University, Nanjing 210098, China, emails: 644503269@qq.com (M. Zhao), 2499737405@qq.com (S. He), 771674813@qq.com (Z. Cao), 107489860@qq.com (W. Chen)*

ABSTRACT

Dissolved organic nitrogen (DON) has been a subject of studies on drinking water treatment because of its potential to form nitrogenous disinfection by-products. Histidine was used in a study on the efficiency and mechanism of amino acid removal in a Fe$_3$O$_4$/oxone (PMS) system. The effects of Fe$_3$O$_4$ dosage, PMS dosage, and pH on the removal efficiency were investigated. The results show that the rates of DON and histidine removal within 1 h in the Fe$_3$O$_4$/PMS system are 45% and 57%, respectively. The optimum pH for histidine degradation is 7, and the optimal dosages of Fe$_3$O$_4$ and PMS are 0.1 g/L and 1.5 mmol/L, respectively. SO$_4^{-\bullet}$ and $^\bullet$OH induced by the transformation of Fe^{2+}–Fe^{3+} on the catalyst surface apparently led to the degradation, indicated by electron spin resonance results, with SO$_4^{-\bullet}$ playing a more important role. The products of the reaction reveal that the part of the histidine was oxidized to NH$_4^+$–N within 60 min and no N$_2$ and NO$_3^-$ formed during the process. Analytical results of high-performance liquid chromatography–mass spectrometry suggest that histidine degradation follows the two separate pathways involving SO$_4^{-\bullet}$ and $^\bullet$OH, but both gradually convert –NH$_2$ into NH$_4^+$–N.

Keywords: Fe$_3$O$_4$; Dissolved organic nitrogen; Histidine; Oxone; Drinking water; Radicals

1. Introduction

Disinfection by-products (DBPs) that result from the treatment of drinking water are a serious concern. Their presence in drinking water was first reported in 1974 [1,2]. Attention should be paid to the formation of nitrogenous disinfection by-products (N-DBPs) because of their greater potential mutagenicity, carcinogenicity, and neurotoxicity [3,4] as compared with those of carbonaceous DBPs such as trihalomethanes, which are well studied and regulated in many countries [5,6]. Dissolved organic nitrogen (DON) is an important part of dissolved organic matter in water. DON mainly refers to a series of compounds containing nitrogen functional groups, including NH, amino groups, cyanide, purine, pyridine, and nitro compounds [7,8]. DON in surface

water is mainly derived from the discharge of urban sewage and agricultural water, soluble bacterial metabolites, metabolites of algae such as blue-green algae, and organic nitrogen present in the soil [9]. DON levels in water harboring algae are higher than those of common water. Protein, free amino acids, and other nitrogenous organic compounds released into a water body, especially in the late stage of an algal outbreak, is the main source of DON in water sources high in algae. Liu et al. [10] and other investigators showed that there are a total of 185 kinds of protein and about 15 main protein types in water samples derived from *Microcystis aeruginosa* cells, occurring at concentrations higher than 0.066 mg/L. Some special types of amino acids are considered as the main precursors of N-DBPs in previous studies [11,12]. Other matter containing DON shows conversion into amino acids during water treatment. We studied the performance and mechanism of histidine removal in a UV/Cu–TiO$_2$

* Corresponding author.

system [13]. Experiments conducted using common amino acids may aid in understanding the reactivity of the amine functional group in catalytic degradation. In this study, histidine was used as the target compound because of its high concentration in raw water and its high potential to form N-DBPs [14,15].

In recent years, advanced oxidation technology based on sulfate radicals ($SO_4^{-\bullet}$) has received much attention from studies on water treatment and in situ chemical oxidation. $SO_4^{-\bullet}$ has a high oxidation potential (E^0 values of +2.5 to +3.1 V) [16], which is close to or greater than that of the hydroxyl radical ($OH^\bullet$; E^0 values of +1.8 to +2.7 V) [17]. $SO_4^{-\bullet}$ can be generated within a large pH range and by several routes such as UV irradiation, transition-metal reactions, and increased temperature [18–22]. Its resistance to oxidation by $^\bullet OH$ in the alkaline range is not very different from that at pH values lower than 7. Furthermore, the residence time of $SO_4^{-\bullet}$ in water is 4 s [23], while that of $OH^\bullet$ is 40 ns [24], which is an advantage for advanced oxidation reactions. $SO_4^{-\bullet}$ can be produced by activating oxone (PMS) and persulfate (PS). Compared with the activation modes for PS, the activation modes for PMS are relatively few. According to recent research [25], PMS can be mainly activated by transition-metal ions and light. However, there are many advantages of using PMS activated by transition-metal ions such as their amenability to ambient temperature and pressure, low energy consumption, as well as non-requirement of a heat source and light source [26]. Consequently, the technology has received much attention.

Fe_3O_4 magnetic nanoparticles have been extensively studied in recent years because of their good stability, easy synthesis and functionalization, high surface area, facile separation by magnetic forces, as well as low toxicity and price [27,28]. These main characteristics make Fe_3O_4 an excellent catalyst for organic reactions [29,30].
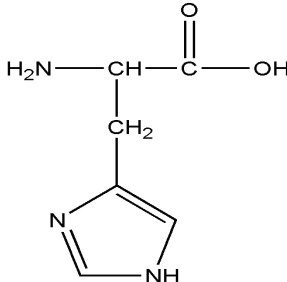
The Fe_3O_4/PMS system is always used to oxidize contaminants in water such as acetaminophen, the azo dye orange G, and aniline [31–33]. However, there have been few studies on using this system to degrade typical amino acids. The main purpose of our research was to investigate the mechanism of removal of typical amino acids in the Fe_3O_4/PMS system and its performance in removal. Histidine was used as model compound for testing catalytic degradation efficiency of the system. The effects of Fe_3O_4 dosage, PMS dosage, and pH on the efficiency of removal were investigated.

2. Materials and methods

2.1. Materials

Reagents were obtained from Sigma-Aldrich Chemical Co., Ltd. (Shanghai, China). All chemicals, which were at least of analytical grade, were used without further purification except when indicated. Methanol (MeOH, HPLC grade) and 5,5-dimethyl-1-pyrrolidine-*N*-oxide (DMPO) were purchased from Sigma-Aldrich Chemical Co., Ltd. and Sigma-Aldrich (Shanghai, China), respectively. Histidine was used because of its great potential for producing haloacetonitriles [34]. Relevant properties of the amino acids are shown in Table 1.

Table 1
Relevant properties of histidine

Amino acid	Histidine
Branched chain	Alkaline
Chemical formula	$C_6H_9N_3O_2$
Molecular weight (g/mol)	155
Chemical structure	

2.2. Analytical methods

NO_3^-, NO_2^-, and NH_4^+ concentrations were measured through a published method [35]. DON content was determined from the difference between the measured total dissolved nitrogen (TDN) content and the sum of measured concentrations of dissolved inorganic nitrogen species by using Eq. (1):

$$\mathrm{DON}\ (\mathrm{mg/L}) = \mathrm{TDN} - \left(NO_3^- - N + NO_2^- - N + NH_4^+ - N \right) \quad (1)$$

Amino acids were analyzed by HPLC using 6-aminoquinolyl-*N*-hydroxysuccinimidyl (AQC) derivatization [36]. The reaction between AQC, amino acids, and ammonia led to the formation of fluorescent complexes, which were separated on an AccQ.Tag Waters (Shanghai, China) C18 HPLC column (3.924 mm × 150 mm) and detected at excitation and emission wavelengths of 240 and 395 nm, respectively. The HPLC system consisted of a Waters TM 600 gradient pump, a Merck (Germany) AS-4000 autosampler, a column heater, and a 474 Waters TM fluorescence detector.

HPLC–MS has been widely used in analytical studies of chemical composition. In the present study, we established a method for the determination of amino acid oxidation products using HPLC–MS. Amino acid oxidation products were identified by ultrahigh-performance liquid chromatography–tandem mass spectrometry (UPLC/MS/MS; Agilent, Waldbronn, Germany). Chromatographic separation was performed at a flow rate of 0.2 mL/min on a Zorbax Eclipse Plus C18 column (2.1 mm × 50 mm, 1.8 μm), which was preceded by a C18 guard column. This column was kept at a temperature of 35°C during the separation period. The mobile phase consisted of a 2 mmol/L ammonium acetate solution (eluent A) and acetonitrile (eluent B) filtered through a membrane with a pore size of 0.22 μm. The injection volume was 5 μL. Detection was performed with an Agilent 6460 series triple quadrupole mass spectrometer equipped with an electrospray ionization source. Qualitative metabolite analysis was conducted with UPLC/MS/MS in full-scan mode. Ion-source parameters were as follows: drying temperature of 300°C, drying flow rate of 5 L/min, nebulizer gas pressure

of 45 psi, sheath-gas temperature of 250°C, sheath-gas flow rate of 5 L/min, capillary voltage of 3,500 V, and nozzle voltage of 500 V.

Electron spin resonance (ESR) experiments were performed using a Bruker EMX-E spectrometer (Germany) with DMPO as a spin-trapping agent.

The surface morphologies of Fe_3O_4 were analyzed by scanning electron microscopy (SEM; Hitachi-S4800, Japan). The surface functional groups were detected by a Fourier transform infrared (FTIR) spectrometer (Tensor 27; Bruker, Germany).

2.3. Experimental procedures

For the catalytic oxidation experiments using the Fe_3O_4/PMS system, the tests were carried out in 250 mL glass brown bottles held in a constant-temperature (25°C ± 1°C) water bath apparatus. In a typical procedure, Fe_3O_4 was added to 200 mL of amino acid solution (10 mg/L), which was then stirred for 60 min to achieve degradation equilibrium. Afterward, the reaction was initiated immediately by adding PMS. At designated time intervals, a 0.5 mL sample was collected from each bottle and immediately filtered through a 0.22 μm membrane. The sample bottles were pre-filled with 0.2 mL of MeOH solution to quench any residual PMS-induced oxidation. Residual water samples were used for the determination of DON. All experiments were performed in triplicate. Data were reported as mean ± standard deviation (SD).

3. Results and discussion

3.1. Characterization of Fe_3O_4

3.1.1. SEM

SEM images of Fe_3O_4 catalysts before and after catalytic degradation of amino acids are shown in Figs. 1(a) and (b), respectively. SEM was carried out to investigate the morphology of the material surface. The catalyst Fe_3O_4 was observed to be mostly scattered before the reaction. Some Fe_3O_4 particles agglomerated after the reaction, thus reducing the surface area and catalytic activity of Fe_3O_4. Similar behavior has been observed in another study [31].

3.1.2. FTIR spectroscopy

Fig. 2 shows FTIR spectra of Fe_3O_4 before and after the reactions. Peaks at 582 cm^{-1} corresponding to the Fe–O group can be clearly observed in the FTIR spectra. The peaks at 1,635 and 3,444 cm^{-1} were, respectively, caused by the bending and stretching vibrations of OH. Similar results have been obtained in Prasad's study [37].

3.1.3. XRD pattern

The structure of Fe_3O_4 (Fig. 3) was analyzed by X-ray powder diffraction (XRD). Peaks of the catalyst appeared at 2θ = 30.1°, 35.6°, 43.2°, 53.7°, 57.2°, and 62.8°, which can be assigned to the (220), (311), (400), (422), (511), and (440) planes, respectively. The XRD pattern matches well with the standard XRD pattern of magnetite (JCPDS no. 19-062) [27].
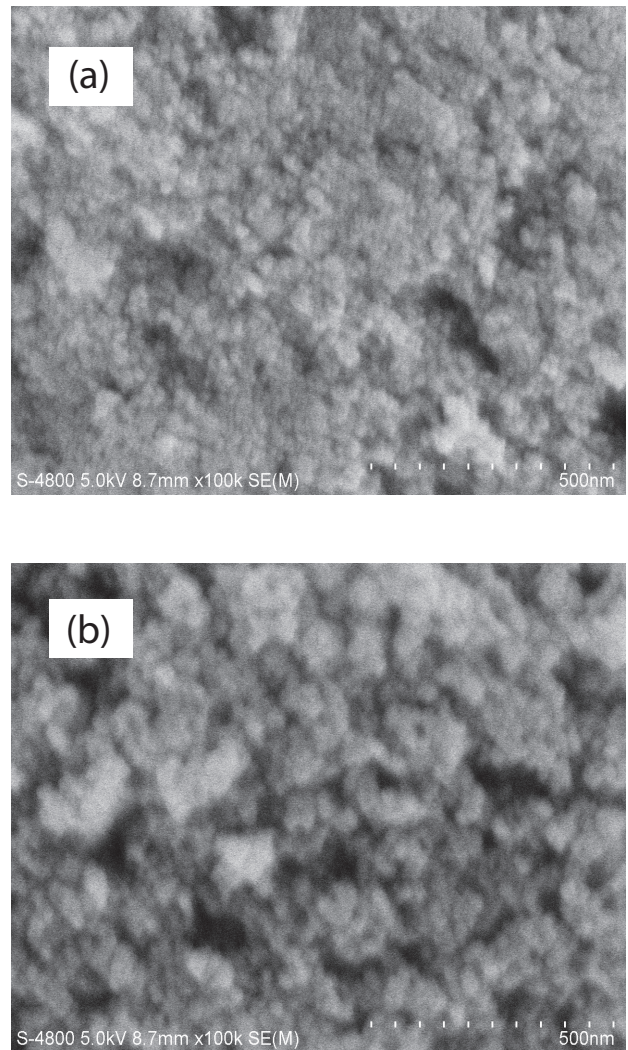

Fig. 1. (a) and (b) SEM images of Fe_3O_4 before and after use, respectively (×100K).
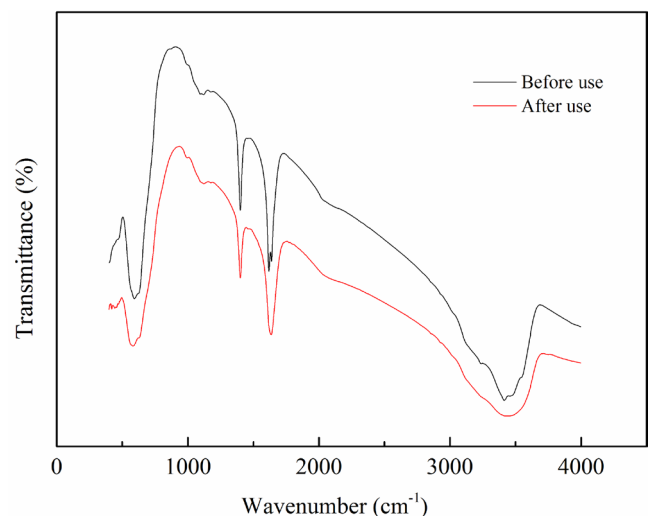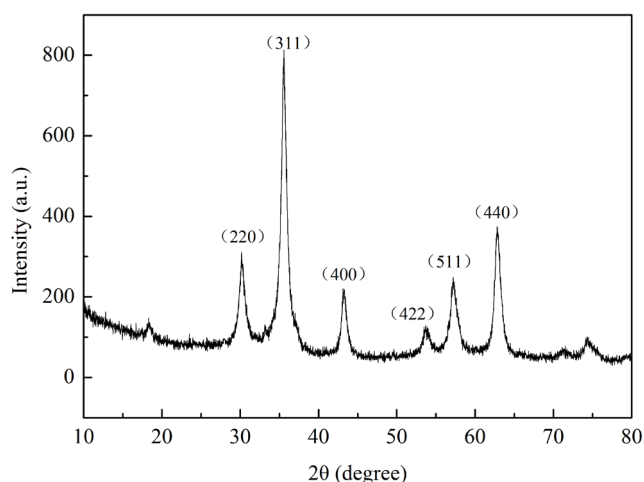

Fig. 2. FTIR of Fe_3O_4 before and after use.

Fig. 3. XRD pattern of Fe_3O_4.

3.2. Degradation efficiency

Fig. 4 depicts the removal of histidine and DON in different reaction systems. The Fe_3O_4/PMS system could catalytically oxidize histidine; the histidine concentration decreased from 10 to 4.3 mg/L within 60 min of the reaction. In contrast, almost no removal occurred in either Fe_3O_4 or PMS system. Transition-metal ions are well-known to catalyze conversion of peroxy-monosulfate to $SO_4^{-\bullet}$, which can oxidize many substances in water, including org-N-rich matters. Results for the removal of DON are similar to those for histidine removal. Under the same reaction conditions, the rate of DON removal was slightly lower than that of histidine removal (45% vs. 57%; Fig. 4). This difference may be explained by the incomplete mineralization of amino acids and thus incomplete transformation to other organic nitrogen matter, which could be detected by DON. The rate of DON removal indicates that part of the DON underwent direct oxidation to inorganic ions.

3.3. Effect of various factors on the catalytic degradation

3.3.1. Effect of Fe_3O_4 dosage

As seen in Fig. 5, the rate of DON removal initially increased and then decreased with the increase in Fe_3O_4 dosage. House [38] and Kolthoff et al. [39] obtained similar results. When the Fe_3O_4 dosage was 0.1 g/L, the rate of DON removal was the highest (45% of DON after 1 h). However, Fe_3O_4 dosages that were too high or too low impeded the reaction. When the Fe_3O_4 dosage is too low, less Fe^{2+} is involved in the reaction, which hardly catalyzes production of $SO_4^{-\bullet}$ from PMS. When the Fe_3O_4 dosage is too high, excess Fe^{2+} reacts with the PMS, resulting in a quenching effect [40]. The optimal Fe_3O_4 dosage was found to be 0.1 g/L.

3.3.2. Effect of PMS dosage

The effect of PMS dosage on amino acid degradation is depicted in Fig. 6. With the increase in PMS concentration, the rate of DON removal generally increased and then decreased. Fig. 5 shows that when the PMS concentration
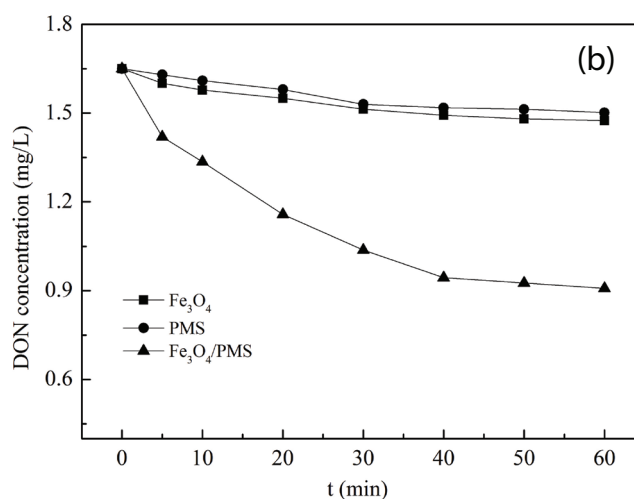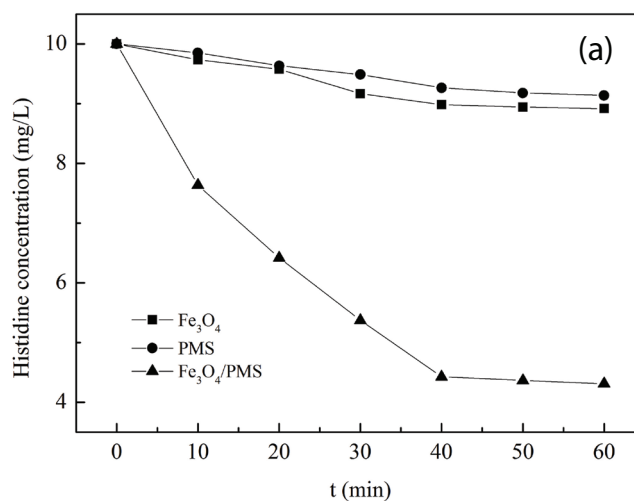
Fig. 4. Degradation efficiency in different systems (a) histidine and (b) DON. Conditions: 0.1 g/L Fe_3O_4; 1 mmol/LPMS; 190 r/min.
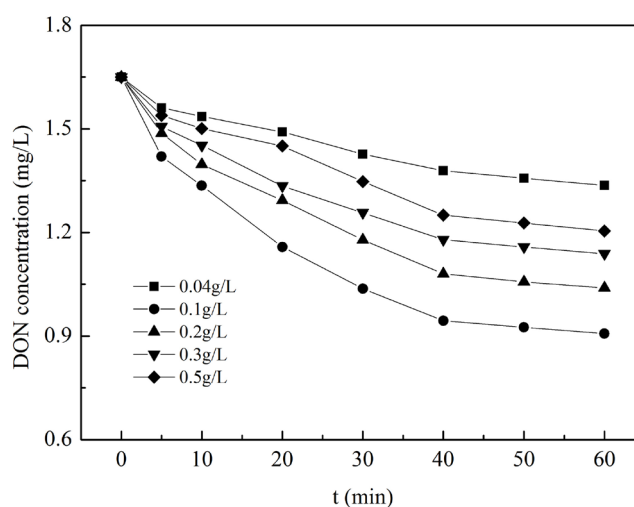
Fig. 5. Effect of Fe_3O_4 dosage on the degradation efficiency. Conditions: 0.04–0.5 g/L Fe_3O_4 (if any); 1 mmol/LPMS; 190 r/min.

increased from 0.2 to 1.5 mmol/L, the DON concentration decreased from 1.65 to 0.87 mg/L; with the PMS concentration further increased to 2 mmol/L, the DON concentration increased to 0.97 mg/L. This trend is due to the sufficient number of active sites of the catalyst when the PMS concentration is low; an increase in PMS concentration in the reaction system can produce more $SO_4^{-\bullet}$, thereby increasing the removal rate of DON from histidine. With further increase in the PMS concentration, however, the equivalent amount of active sites on the Fe_3O_4 surface become saturated, thus increasing the amount of PMS that is not involved in the reaction for $SO_4^{-\bullet}$ production. Similar inhibition has been reported in the literature [41]. Therefore, the optimal PMS dosage is 1.5 mmol/L. Moreover, the best Fe_3O_4/PMS molar ratio is 4:15 (Figs. 5 and 6).

3.3.3. Effect of initial pH

The pH of raw water changes with the climate as well as with the growth of plankton and, especially, growth of algae and aquatic plants. The pH not only affects the electriferous state of the Fe_3O_4 surface, but it also modifies the ionization degree of the target compound in the reaction system. Therefore, determining the effect of pH on the catalytic oxidation efficiency is necessary. The effect of pH on amino acid degradation is presented in Fig. 7. The figure shows that the DON removal rate increases first and then decreases with the increase in pH, reaching 47% at pH 7. The rate of removal of organic matter with PMS was higher when the pH was between 4 and 9. Since the isoelectric point of Fe_3O_4 is 5.0, the surface charge is negative when the pH is >5, and it is positive when the pH is <5. However, when the pH is >5, the Fe^{2+} surface is negatively charged, repelling negative ions produced by PMS dissolution and leading to a decreased rate of DON removal. In an acidic environment (pH of <5), hydrogen bonding between H^+ and O produced by the dissolution of PMS is favorable, thereby inhibiting the catalytic oxidation. Therefore, the optimal pH value is 7. Similar results were also obtained in the study of Pignatello et al. [42].
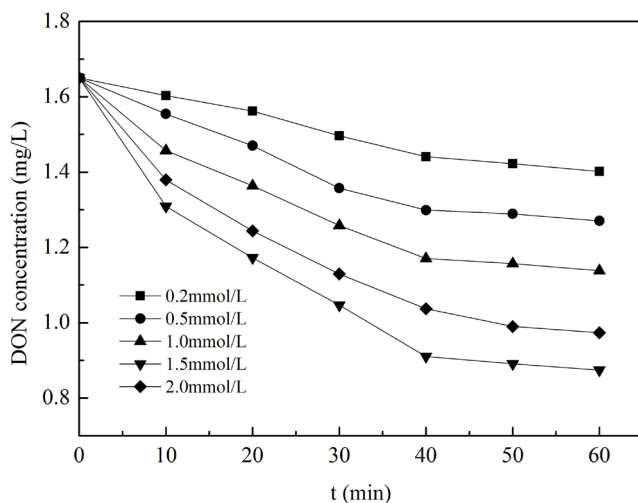
3.4. Stability and reusability of Fe_3O_4

To evaluate the stability of the nanocatalysts Fe_3O_4, the leaching of Fe^{3+} was monitored during PMS oxidation of amino acids in the presence of catalyst at 0.1 g/L concentration (initial histidine concentration = 10 mg/L, pH = 7.0, and PMS concentration = 1.5 mmol/L). Inductively coupled plasma mass spectrometry results indicate that the concentration of Fe^{3+} leached from the nanocatalysts was below the detection limit (0.05 µg/L), suggesting that Fe_3O_4 is stable during the catalytic degradation reactions. As the Fe_3O_4 and PMS dosages were increased by 10 times (i.e., 1.0 g/L catalyst and 15 mmol/L PMS), the concentration of Fe^{3+} leached was <3.2 µg/L (Fig. 8). Moreover, FTIR spectra of Fe_3O_4 before and after use are identical (Fig. 2), indicating that Fe_3O_4 is stable during the reaction.

The Fe_3O_4 catalysts were collected and recycled for five times. As seen in Fig. 9, the rate of DON removal in each
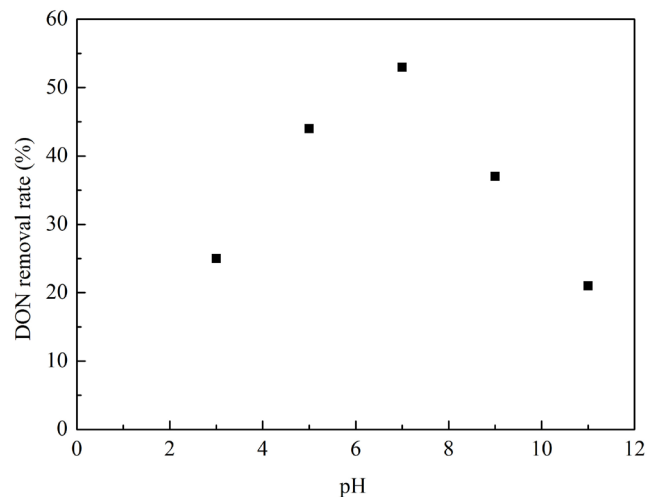
Fig. 7. Effect of pH value on the degradation efficiency. Conditions: 0.1 g/L Fe_3O_4; 1.5 mmol/LPMS; 190 r/min.
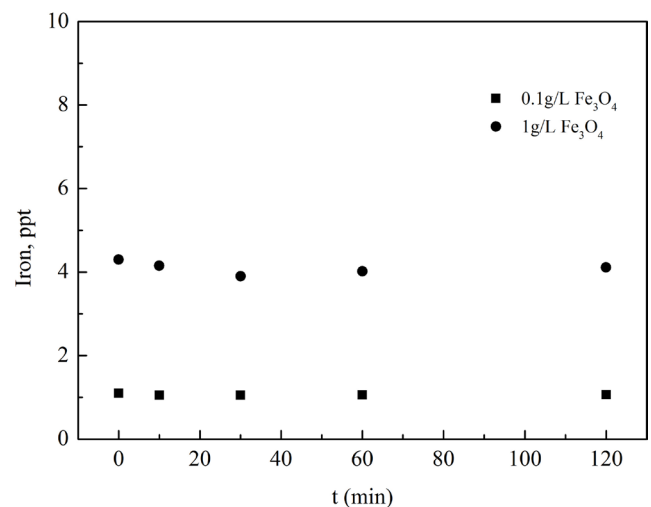
Fig. 6. Effect of PMS dosage on the degradation efficiency. Conditions: 0.1 g/L Fe_3O_4; 0.2–2.0 mmol/LPMS (if any); 190 r/min.

Fig. 8. Fe leaching in Fe_3O_4/PMS system. Conditions: 0.1 g/L Fe_3O_4; 1.5 mmol/LPMS; 1 g/L Fe_3O_4; 15 mmol/LPMS; 190 r/min.

cycle gradually decreased. The removal rates within 60 min were 47%, 40%, 28%, and 25% for the first, second, third, and fourth runs, respectively. The Fe_3O_4 catalysts agglomerated during the reaction, and the surface area of the materials decreased substantially, leading to a reduction of degradation efficiency (Figs. 1(a) and (b)). Moreover, the amount of Fe(II) decreased after conversion to Fe(III); thus, the catalyst efficiency decreased upon reuse.

3.5. Proposed mechanisms

3.5.1. Behaviors of radicals during oxidation

Several radical scavengers were used to identify the main functional groups in the system. MeOH is an alcohol containing alpha hydrogen (a-H), which can quickly quench $OH^•$ and $SO_4^{-•}$ by reacting with them. *tert*-Butyl alcohol (TBA) does not contain a-H, and it can react rapidly with $OH^•$ only; its reaction with $SO_4^{-•}$ is much slower. A previous study has revealed that [43] the rates of reaction of MeOH with $SO_4^{-•}$ and $OH^•$ are 1.6×10^9–7.7×10^9 min^{-1} and 1.2×10^9–2.8×10^9 min^{-1}, respectively. The two reaction systems are thus not very different. However, the rate of reaction of TBA with $SO_4^{-•}$ is 4.0×10^5–9.1×10^5 min^{-1}, and that of the reaction of TBA with $OH^•$ is 3.8×10^8–7.6×10^8 min^{-1}, a difference of nearly 1,000 times. The type of free radical in the reaction system can be determined from the difference in reaction rate. Results for the quenching agents are shown in Fig. 10. Without any quenching agent, approximately 47% of the DON was removed in 60 min. However, the histidine degradation rate clearly dropped by 12% and 28% within 60 min in the presence of 0.02 M TBA and 0.02 M MeOH, respectively. Compared with the drop in DON removal rate in the presence of TBA, the drop was substantial in the presence of MeOH, indicating that $SO_4^{-•}$ as oxidizing species mainly formed during the activated decomposition of PMS by Fe_3O_4.

Qualitative analysis was carried out on free radicals and $SO_4^{-•}$ by ESR in Fig. 11, • represents $OH^•$ and ★ represents $SO_4^{-•}$. $OH^•$ and $SO_4^{-•}$ could be determination from the signals of DMPO–OH adducts and DMPO–SO_4 adducts, respectively.

We detected $SO_4^{-•}$, which has the hyperfine splitting constants a_N = 13.2 G, a_H = 9.6 G, a_H = 1.48 G, and a_H = 0.78 G, along with $OH^•$. These results suggest that both radical species formed, similar to the results of previous studies [44,45]. Fig. 11 shows that the Fe_3O_4 system does not generate free radicals. However, the PMS system had $OH^•$ and $SO_4^{-•}$, albeit at levels lower than those in the Fe_3O_4/PMS system. The peak height reflects the amount of free radicals. ESR thus confirmed that $OH^•$ and $SO_4^{-•}$ can form in the Fe_3O_4/PMS system, with $SO_4^{-•}$ playing a more important role.

3.5.2. Degradation pathway

To confirm the extent of DON oxidation in water, the concentrations of TDN, as well as those nitrogen from ammonium (NH_4^+), nitrite (NO_3^-), and nitrate (NO_2^-), were determined at different reaction times (results are shown in Fig. 12). The main forms of nitrogen showed different variation tendencies (Fig. 12). The DON concentrations decreased whereas the NH_4^+ concentration increased. No obvious change in the TDN, NO_3^-, and NO_2^- nitrogen concentration was detected during the entire oxidation process. According to the variation value of DON and NH_4^+ (1.65 vs. 0.87 mg/L and 0.043 vs. 0.58 mg/L), the increase in NH_4^+ nitrogen concentration is caused by histidine oxidation and that the NH_4^+ was not converted to nitrogen. These results are contrary to those in our former study [13], in which histidine was completely degraded to NH_4^+ and NO_3^- first, with NO_3^- was finally being reduced to N_2 and remove from water by a UV/Cu–TiO_2 system. This result may be attributed to the fact that photocatalytic oxidation is a coupling reaction; that is, doping with copper ion could improve the ability to oxidize certain compounds in water [7] and enhance the efficiency of reduction of nitrate to N_2 and the performance in TN degradation by photocatalyzed reaction [46]. However, the Fe_3O_4/PMS system is a heterogeneous catalytic oxidation, and there is no interaction between NH_4^+ and NO_3^- in the reaction process.

HPLC–MS was used to identify the intermediates and final products of amino acid oxidation. According to previous
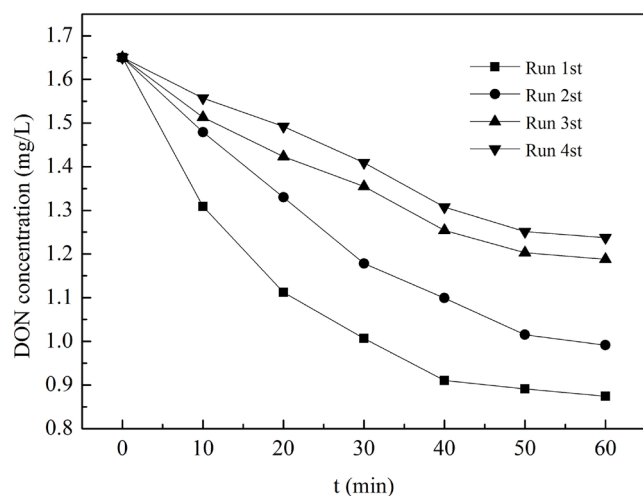
Fig. 9. Effect of catalyst recycle number on the degradation efficiency. Conditions: 0.1 g/L Fe_3O_4; 1.5 mmol/LPMS; 190 r/min.
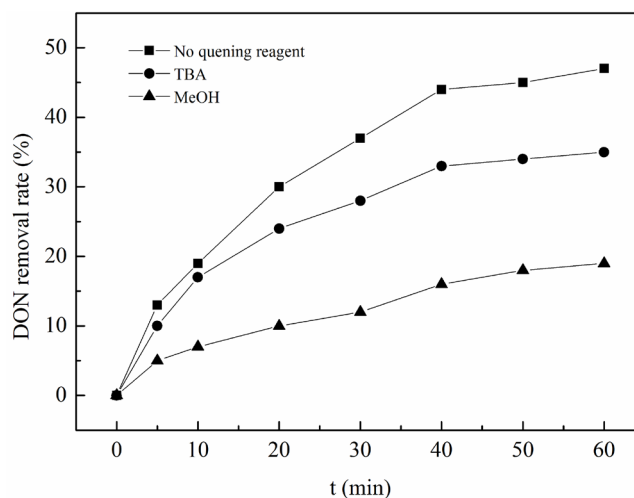
Fig. 10. Effect of different radicals scavengers on the degradation of histidine. Conditions: 0.1 g/L Fe_3O_4; 1.5 mmol/LPMS; 190 r/min.
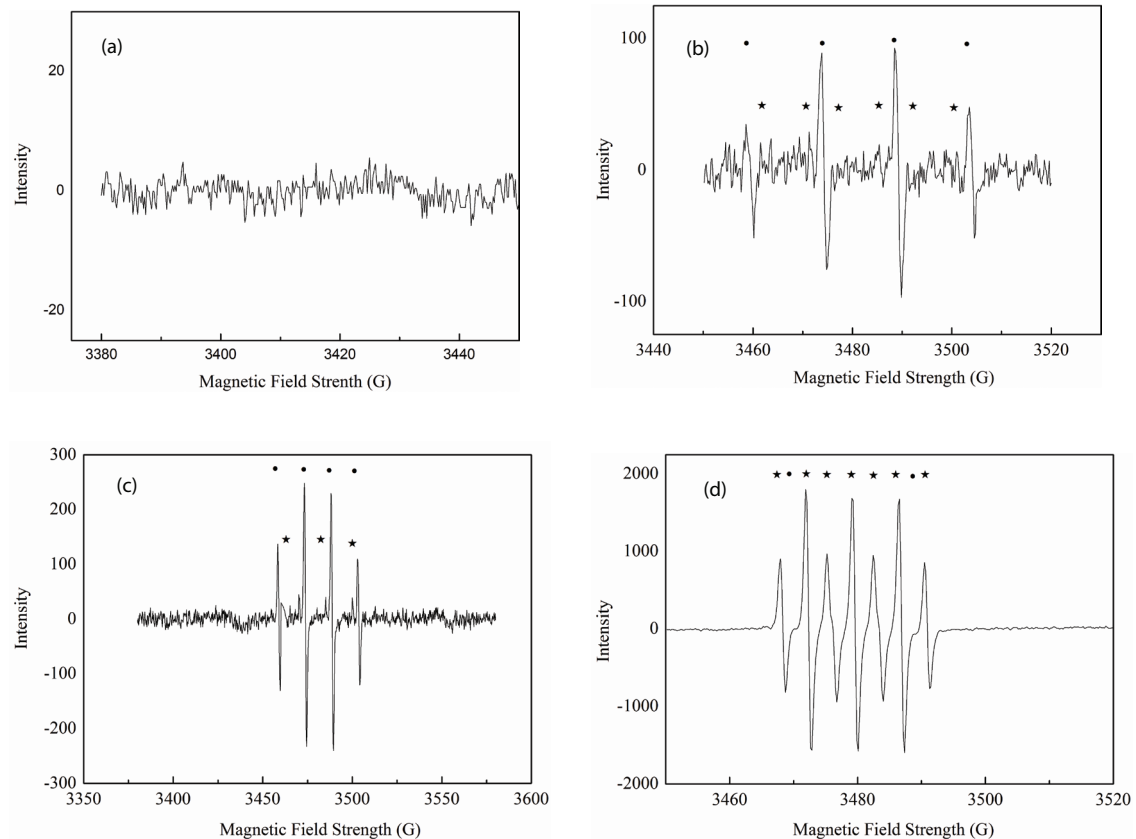
Fig. 11. ESR spectra obtained for (a) Fe_3O_4; (b) PMS; (c) $t = 2$ min, Fe_3O_4/PMS system; and (d) $t = 10$ min, Fe_3O_4/PMS system. Conditions: 1.0 g/L Fe_3O_4; 1.5 mmol/LPMS; [DMPO] = 0.1 M; ● represents OH• and ★ represents SO_4^-•.
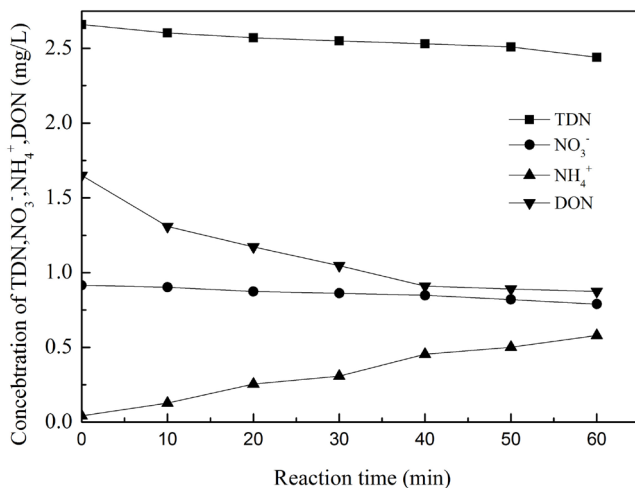
Fig. 12. Changes of TDN, NO_3^-, NH_4^+ in the DON degradation in the Fe_3O_4/PMS system.

Fig. 13. Mass spectrum of histidine-containing water sample after the catalytic treatment.

studies [47,48], the amino and carboxyl groups can be simultaneously removed, with carboxylic acid consequently generated in the presence of the catalyst. However, the recovery rate of carboxylic acid was low. Thus, the specific oxidation process is as follows.

After catalytic treatment, water samples with amino acid were analyzed by HPLC–MS (spectra are shown in Fig. 13).
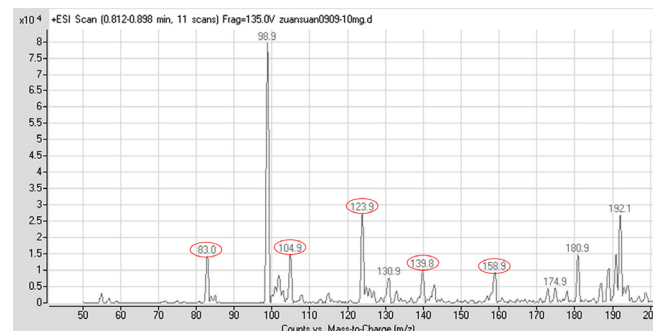
Fig. 13 shows that the main mass-to-charge ratios (m/z) for the mass spectrum of the histidine-containing water sample after catalytic treatment are 158.9, 139.8, and 104.9. The molecular formula of these substances could be tentatively identified on the basis of the m/z ratios and the amino acid structure (Table 2).

The aforementioned figures and Table 2 describe oxidative decarboxylation during deamination of histidine.

As shown in Fig. 14, histidine undergoes degradation via two processes under the action of two radicals within 60 min. The carboxyl group of the amino acid undergoes protonation, forming the carboxyl anion. In the first process, carboxyl

Table 2
Identification of amino acid oxidation products

Amino acid	Monitoring ion	m/z	Molecular formula
Histidine	[M + Na]+	158.9	$C_6H_9N_3O_2$
	[M + H]+	139.8	CH_2SO_4
	[M + H]+	123.9	$C_5H_9N_3$
	[M + H]+	104.9	$C_3H_5O_4$
	[M + H]+	83.0	$C_4H_{10}N_2$

anion is oxidized to carboxyl radical by $SO_4^{-•}$. The α-amino free radical can convert to α-amino carbonium ion, forming the protonated imine. Finally, the carboxylic acid can form by catalytic degradation. In the other process, carboxyl anion is oxidized to 4-methylimidazole or isomers of 4-methyl by $^•OH$. This reaction is similar to that in a previous study [48]. 4-Methylimidazole is an important constituent of caramel pigment, and a compound that is commonly used in pharmaceuticals, as in the synthesis of antibacterial agents, as the main raw material. Its use in the manufacture of cimetidine, an inhibitor of gastric acid secretion, is common. It is also used in the
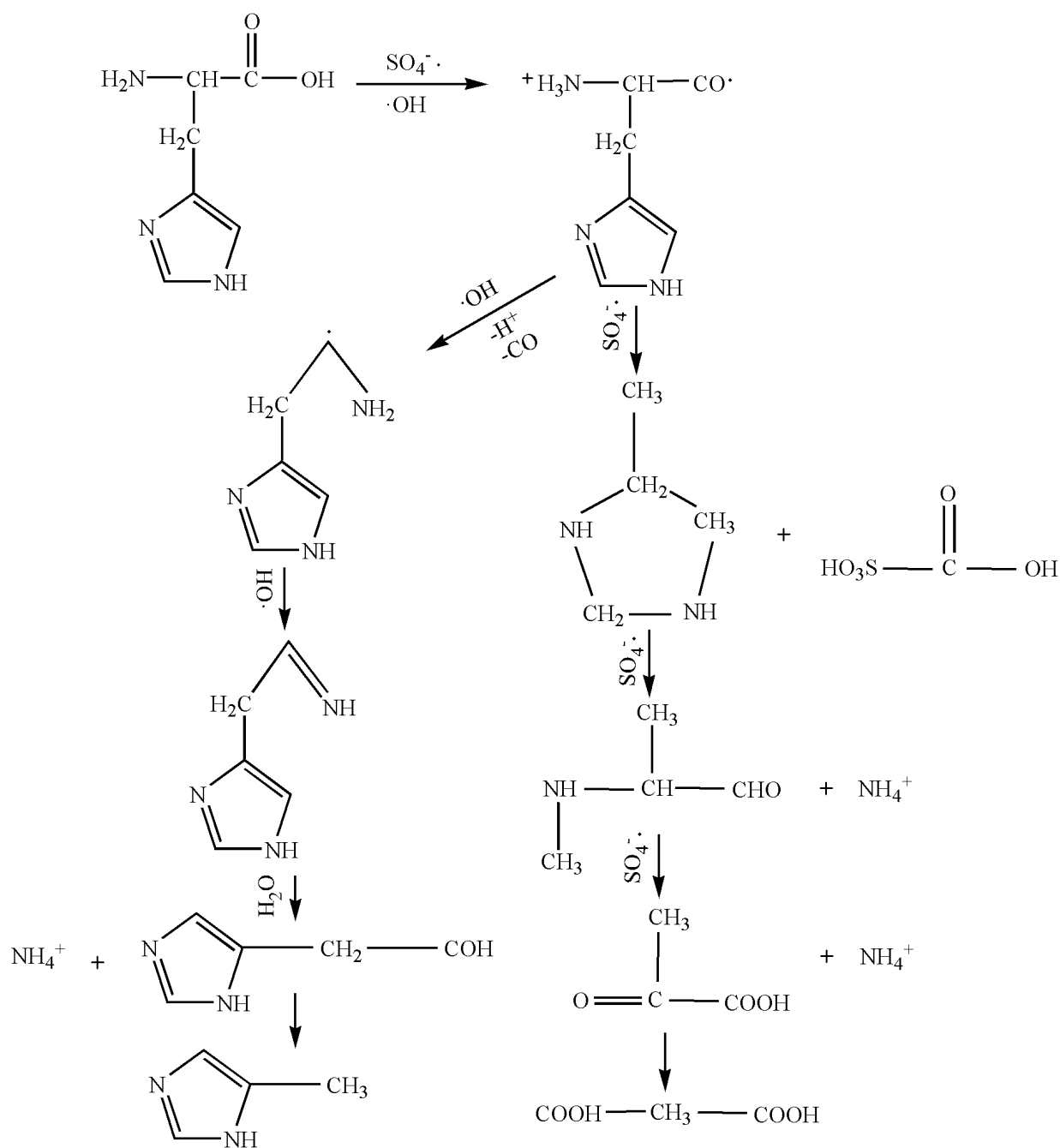

Fig. 14. Degradation pathways of histidine in the Fe_3O_4/PMS system. Conditions: 0.1 g/L Fe_3O_4; 1.5 mmol/LPMS; 190 r/min; t = 60 min.

manufacture of curing agents, preservatives, and agricultural chemicals. The mass spectra in Fig. 13 suggest that the response value of 4-methylimidazole is very low. The concentrations of DON and histidine decreased (Figs. 4 and 14). Their removal was not complete, showing that there is a part of the process of nitrogen removal. Some studies [14,15] have indicated that histidine is a precursor of N-DBPs; that is, the decrease in DON and histidine concentrations can be varied to control the formation potential of N-DBPs. The formation potential of the intermediate product remains unclear. According to Chu's study [49], UV/PS pre-treatment is effective at reducing the formation of dichloroacetonitrile during subsequent chlorination, despite similar oxidation pathways between the UV/PS and Fe_3O_4/PMS. Therefore, histidine degradation in the Fe_3O_4/PMS system can reduce the formation of N-DBPs.

4. Conclusions

This study is the first that uses Fe_3O_4 as a heterogeneous catalyst for activating PMS in the degradation of N-DBPs. Our results show that Fe_3O_4 can effectively catalyze PMS for the degradation of DON. Under all the experimental conditions applied, the removal rate of DON from histidine in the Fe_3O_4/PMS system within 60 min is 47%. The optimum pH for histidine degradation is 7. Optimal dosages of Fe_3O_4 and PMS are 0.1 g/L and 1.5 mmol/L, respectively. During the reaction, the catalyst is stable and does not cause any significant leaching of iron into water. ESR results show that Fe^{2+}–Fe^{3+} conversion leads to radical generation. Both $OH^{\bullet}$ and $SO_4^{-\bullet}$ were detected in the system. Therefore, DON degradation is a result of oxidation by both radicals.

Acknowledgments

References

[1] J.J. Rook, Formation of haloforms during chlorination of natural water, J. Water Treat. Exam., 23 (1973) 234–243.

[2] T.A. Bellar, J.J. Lichtenberg, R.C. Kroner, The occurrence of organohalides in chlorinated drinking water, J. Am. Water Works Assoc., 66 (1974) 703–706.

[3] R.J. Bull, L.S. Birnbaum, K.P. Cantor, J.B. Rose, B.E. Butterworth, R. Pegram, J. Tuomisto, Water chlorination: essential process or cancer hazard?, Fundam. Appl. Toxicol., 28 (1995) 155–166.

[4] S.D. Richardson, M.J. Plewa, E.D. Wagner, R. Schoeny, D.M. Demarini, Occurrence, genotoxicity, and carcinogenicity of regulated and emerging disinfection by-products in drinking water: a review and roadmap for research, Mutat. Res./Rev. Mutat. Res., 636 (2007) 178–242.

[5] W. Chu, D. Li, N. Gao, M.R. Templeton, C. Tan, Y. Gao, The control of emerging haloacetamide DBP precursors with UV/persulfate treatment, Water Res., 72 (2015) 340–348.

[6] W. Chu, C. Li, N. Gao, M.R. Templetonb, Y. Zhang, Terminating pre-ozonation prior to biological activated carbon filtration results in increased formation of nitrogenous disinfection by-products upon subsequent chlorination, Chemosphere, 121 (2015) 33–38.

[7] C. Liu, J. Wang, W. Chen, H. Zhu, H. Bi, Characterization of DON in IOM derived from *M. aeruginosa* and its removal by sunlight/immobilized TiO_2 system, RSC Adv., 5 (2015) 41203–41209.

[8] C. Liu, S. Li, S. Gong, S. Yuan, X. Yu, Mixing regime as a key factor to determine DON formation in drinking water biological treatment, Chemosphere, 139 (2015) 638–643.

[9] W. Chu, N. Gao, D. Yin, Y. Deng, M.R. Templeton, Ozone–biological activated carbon integrated treatment for removal of precursors of halogenated nitrogenous disinfection by-products, Chemosphere, 86 (2012) 1087–1091.

[10] C. Liu, J. Wang, W. Chen, C. Dong, C. Li, The removal of DON derived from algae cells by Cu-doped TiO_2 under sunlight irradiation, Chem. Eng. J., 280 (2015) 588–596.

[11] I.K. Konstantinou, T.A. Albanis, TiO_2-assisted photocatalytic degradation of azo dyes in aqueous solution: kinetic and mechanistic investigations: a review, Appl. Catal., B, 49 (2004) 1–14.

[12] C.S. Uyguner-Demirel, M. Bekbolet, Significance of analytical parameters for the understanding of natural organic matter in relation to photocatalytic oxidation, Chemosphere, 84 (2011) 1009.

[13] C. Liu, J. Wang, W. Chen, Z. Sun, Z. Cao, Performance and mechanism of UV/immobilized Cu-TiO_2 system to degradation histidine, J. Nanomater., 2016 (2016) 1–9.

[14] X. Yang, Q. Shen, W. Guo, J. Peng, Y. Liang, Precursors and nitrogen origins of trichloronitromethane and dichloroacetonitrile during chlorination/chloramination, Chemosphere, 88 (2012) 25–32.

[15] A. Dotson, P. Westerhoff, Occurrence and removal of amino acids during drinking water treatment, J. Am. Water Works Assoc., 101 (2009) 101–115.

[16] P. Neta, R.E. Huie, A.B. Ross, Rate constants for reactions of inorganic radicals in aqueous solution, J. Phys. Chem. Ref. Data, 17 (1988) 1027–1284.

[17] G.V. Buxton, C.L. Greenstock, W.P. Helman, A.B. Ross, Critical review of rate constants for reactions of hydrated electrons chemical kinetic data base for combustion chemistry, J. Phys. Chem. Ref. Data, l7 (1988) 513–780.

[18] C.S. Liu, K. Shih, C.X. Sun, F. Wang, Oxidative degradation of propachlor by ferrous and copper ion activated persulfate, Sci. Total Environ., 416 (2012) 507–512.

[19] J.A. Khan, X. He, N.S. Shah, H.M. Khan, E. Hapeshi, D.F. Kassinos, D.D. Dionysiou, Kinetic and mechanism investigation on the photo chemical degradation of atrazine with activated H_2O_2, $S_2O_8^{2-}$ and HSO_5^-, Chem. Eng. J., 252 (2014) 393–403.

[20] G.P. Anipsitakis, D.D. Dionysiou, Radical generation by the interaction of transition metals with common oxidants, Environ. Sci. Technol., 38 (2004) 3705–3712.

[21] M.G. Antoniou, A.A.D.L. Cruz, D.D. Dionysiou, Degradation of microcystin-LR using sulfate radicals generated through photolysis, thermolysis and e−, transfer mechanisms, Appl. Catal., B, 96 (2010) 290–298.

[22] B. Petri, In situ chemical oxidation of contaminated soil and groundwater using persulfate: a review, Crit. Rev. Environ. Sci. Technol., 40 (2010) 55–91.

[23] M. Banerjee, R.S. Konar, Comment on the paper "Polymerization of acrylonitrile initiated by $K_2S_2O_8$-Fe(II) redox system", J. Polym. Sci., Part A, 22 (1984) 1193–1195.

[24] A. Georgi, F.D. Kopinke, Interaction of adsorption and catalytic reactions in water decontamination processes: part I. Oxidation of organic contaminants with hydrogen peroxide catalyzed by activated carbon, Appl. Catal., B, 58 (2005) 9–18.

[25] B. Wang, Progress in advanced oxidation processes based on sulfate radical, Environ. Eng., 30 (2012) 53–57.

[26] J. Zhang, M. Chen, L. Zhu, Activation of peroxymonosulfate by iron-based catalysts for orange G degradation: role of hydroxylamine, RSC Adv., 6 (2016) 47562–47569.

[27] A.M. Malekzadeh, S. Shokrollahi, A. Ramazani, S.J.T. Rezaei, P.A. Asiabi, S.W. Joo, Synthesis of hexabenzylhexaazaisowurtzitane (HBIW) under ultrasound irradiation with Fe_3O_4@PCA nanoparticles as an efficient and reusable nanomagnetic catalyst, Cent. Eur. J. Energetic Mater., 14 (2017) 336–350.

[28] M. Khoobi, M. Khalilvand-Sedagheh, A. Ramazani, Z. Asadgol, H. Forootanfar, M.A. Faramarzi, Synthesis of polyethyleneimine (PEI) and β-cyclodextrin grafted PEI nanocomposites with magnetic cores for lipase immobilization and esterification, J. Chem. Technol. Biotechnol., 91 (2016) 375–384.

[29] S. Taghavi Fardood, A. Ramazani, Z. Golfar, S.W. Joo, Green synthesis of Ni-Cu-Zn ferrite nanoparticles using tragacanth gum and their use as an efficient catalyst for the synthesis of polyhydroquinoline derivatives, Appl. Organomet. Chem., 82 (2017) e3823.

[30] N. Dayyani, A. Ramazani, S. Khoee, A. Shafiee, Synthesis and characterization of the first generation of polyamino-ester dendrimer-grafted magnetite nanoparticles from 3-aminopropyltriethoxysilane (APTES) via the convergent approach, Silicon, (2017) 1–7. DOI: 10.1007/s12633-016-9497-6.

[31] C. Tan, N. Gao, Y. Deng, J. Deng, S. Zhou, J. Li, X. Xin, Radical induced degradation of acetaminophen with Fe_3O_4 magnetic nanoparticles as heterogeneous activator of peroxymonosulfate, J. Hazard. Mater., 276 (2014) 452–460.

[32] X.R. Xu, X.Z. Li, Degradation of azo dye Orange G in aqueous solutions by persulfate with ferrous ion, Sep. Purif. Technol., 72 (2010) 105–111.

[33] Y.Q. Zhang, W.L. Huang, D.E. Fennell, In situ chemical oxidation of aniline by persulfate with iron(II) activation at ambient temperature, Chin. Chem. Lett., 21 (2010) 911–913.

[34] H. Ueno, T. Moto, Y. Sayato, K. Nakamuro, Disinfection by-products in the chlorination of organic nitrogen compounds: by-products from kynurenine, Chemosphere, 33 (1996) 1425–1433.

[35] State Environmental Protection Administration of China, Monitoring and Analysis Methods of Water and Wastewater, 4th ed., China Environmental Science Press, Beijing, 2002.

[36] J. Díaz, J.L. Lliberia, L. Comellas, F. Broto-Puig, Amino acid and amino sugar determination by derivatization with 6-aminoquinolyl-N-hydroxysuccinimidyl carbamate followed by high-performance liquid chromatography and fluorescence detection, J. Chromatogr., A, 719 (1996) 171–179.

[37] C. Prasad, G. Yuvaraja, P. Venkateswarlu, Biogenic synthesis of Fe_3O_4 magnetic nanoparticles using *Pisum sativum*, peels extract and its effect on magnetic and Methyl orange dye degradation studies, J. Magn. Magn. Mater., 424 (2016) 376–381.

[38] D.A. House, Kinetics and mechanism of oxidations by peroxydisulfate, Chem. Rev., 62 (1961) 185–203.

[39] I.M. Kolthoff, A.I. Medalia, H.P. Raaen, The reaction between ferrous iron and peroxides. IV. Reaction with potassium persulfate, J. Am. Chem. Soc., 73 (1951) 1733–1739.

[40] H. Lin, J. Wu, H. Zhang, Degradation of clofibric acid in aqueous solution by an $EC/Fe^{3+}/PMS$ process, Chem. Eng. J., 244 (2014) 514–521.

[41] X. Chen, J. Chen, X. Qiao, D. Wang, X. Cai, Performance of nano-Co_3O_4/peroxymonosulfate system: kinetics and mechanism study using Acid Orange 7 as a model compound, Appl. Catal., B, 80 (2008) 116–121.

[42] J.J. Pignatello, E. Oliveros, A. MacKay, Advanced oxidation processes for organic contaminant destruction based on the Fenton reaction and related chemistry, Crit. Rev. Environ. Sci. Technol., 36 (2006) 1–84.

[43] J. Zhao, Y. Zhang, X. Quan, S. Chen, Enhanced oxidation of 4-chlorophenol using sulfate radicals generated from zero-valent iron and peroxydisulfate at ambient temperature, Sep. Purif. Technol., 71 (2010) 302–307.

[44] C. Tan, N. Gao, W. Chu, C. Li, M.R. Templeton, Degradation of diuron by persulfate activated with ferrous ion, Sep. Purif. Technol., 95 (2012) 44–48.

[45] G.P. Anipsitakis, D.D. Dionysiou, Degradation of organic contaminants in water with sulfate radicals generated by the conjunction of peroxymonosulfate with cobalt, Environ. Sci. Technol., 37 (2003) 4790.

[46] H. Kominami, A. Furusho, S.Y. Murakami, H. Inoue, Y. Kera, B. Ohtani, Effective photocatalytic reduction of nitrate to ammonia in an aqueous suspension of metal-loaded titanium(IV) oxide particles in the presence of oxalic acid, Catal. Lett., 76 (2001) 31–34.

[47] A.O. Allen, C.J. Hochanadel, J.A. Ghormley, T.W. Davis, Decomposition of water and aqueous solutions under mixed fast neutron and γ-radiation, J. Phys. Chem., 56 (1951) 575–586.

[48] W. Chu, J. Hu, T. Bond, N. Gao, B. Xu, D. Yin, Water temperature significantly impacts the formation of iodinated haloacetamides during persulfate oxidation, Water Res., 98 (2016) 47–55.

[49] W. Chu, D. Li, Y. Deng, N. Gao, Y. Zhang, Y. Zhu, Effects of UV/PS and UV/H_2O_2 pre-oxidations on the formation of trihalomethanes and haloacetonitriles during chlorination and chloramination of free amino acids and short oligopeptides, Chem. Eng. J., 301 (2016) 65–72.